



Universiteit  
Leiden  
The Netherlands

## On periodically driven quantum systems

Tarasinski, B.M.

### Citation

Tarasinski, B. M. (2016, September 20). *On periodically driven quantum systems. Casimir PhD Series*. Retrieved from <https://hdl.handle.net/1887/43150>

Version: Not Applicable (or Unknown)

License:

Downloaded from: <https://hdl.handle.net/1887/43150>

**Note:** To cite this publication please use the final published version (if applicable).

Cover Page



Universiteit Leiden



The handle <http://hdl.handle.net/1887/43150> holds various files of this Leiden University dissertation.

**Author:** Tarasinski, B.M.

**Title:** On periodically driven quantum systems

**Issue Date:** 2016-09-20

# 1 Introduction

## 1.1 Preface

In the last few decades, a major part of the field of condensed matter physics is the exploration, classification, prediction and experimental realization of *topological insulators and superconductors* (which, perhaps counter-intuitively, can be treated very similarly; this is because superconductors are *thermal* insulators). Such materials are indistinguishable from “normal” (or *trivial*) insulators or superconductors in local bulk properties like density of states or electrical and thermal conductivity, but are still different from normal states in a manner that disallows a transition from topological to trivial without going through a *topological phase transition*, during which the material loses its insulating property.<sup>75,143</sup>

A principle called *bulk-boundary correspondence* implies that a boundary between two different topological phases hosts robust edge states, often with very peculiar properties, like absence of backscattering or dephasing, or non-Abelian exchange statistics. These properties have been recognized to have potential applications in quantum computing, both as memory and for the implementation of quantum gates.<sup>131</sup>

Since then, a lot of experimental effort was put in the realization and manipulation of materials with topological phases, but the materials shown to have such properties are rather sparse.

In search for new experimental handles to engineer the topological properties of a material, the possibility of periodic external driving was proposed,<sup>116</sup> which was shown to induce a topological band structure in an initially trivial semiconductor. When periodical driving is introduced to a quantum system, the so-called *Floquet theory* is usually employed, so that this new type of topological insulators are called *Floquet topological insulators*.

A model that captures the essential difference between insulators and Floquet insulators is the so-called *quantum walk*, a quantum-mechanical

## 1 Introduction

analogue to the random walk. Just like the classical random walk, the quantum walk evolves in discrete time steps, so that the effect of the external driving is represented by the subsequent application of time-step evolution operators. It turns out that the family of quantum walks are rich enough to implement relatively simple models with non-trivial phase diagram for all different possible symmetry classes.<sup>101</sup> Quantum walks thus can serve as a platform to study the different topological phases of Floquet topological insulators.

Besides their topological properties, quantum walks have also gained a lot of popularity in the design of quantum algorithms.<sup>91,175</sup> As many classical algorithms can be understood as a (more or less) random walk on a decision graph, the “quantization” of that random walk may lead to a quantum algorithm for the same problem, often achieving close to optimal quantum speed-up.

In the next three chapters of this thesis, we study the properties of Floquet topological insulators by the help of quantum walks. In the chapter thereafter, we present a related but slightly different study: We consider the time-dependent transition of a (non-Floquet) topological Josephson junction and its relaxation to the new ground state. The final chapter is devoted to the experimental study of the spin-orbit interaction in nanowires of indium antimonide, which are the central building block in one of the most promising experimental approaches to manufacture a one-dimensional topological superconductor.<sup>128</sup>

In the rest of this introduction, we outline a few basic ideas that are used heavily in this thesis, especially the next three chapters, introducing most of the key concepts highlighted above, including the Floquet theory, basic properties of quantum walks, the idea of band topology and the resulting bulk-boundary correspondence, and a connection between a quantum walk-based algorithm and band topology. We conclude with a more detailed summary of the subsequent chapters of this thesis.

## 1.2 Floquet formalism

*Periodically driven systems* Most chapters in this thesis are concerned with non-interacting single quantum particles whose time evolution is governed by explicitly time-dependent Hamiltonians. Especially, we consider a time evolution where the system is subject to a *periodic driving*, so that the Hamiltonian is explicitly dependent on time and

obeys

$$H(t) = H(t + T) \quad (1.1)$$

for some fixed period  $T$ .

The energy of such systems is not conserved and it is not possible to reduce the Schrödinger equation to the stationary Schrödinger equation. However, the situation is essentially equivalent to the situation of a particle in a periodic potential, implying broken translational invariance in *space*, which can be tackled by the well-known Bloch theorem. Here, similar ideas can be applied, replacing space with *time*. The resulting theory is referred to as the *Floquet theory* of periodically driven systems.

*The Floquet operator* The basic element of Floquet theory is the unitary *Floquet operator*  $F$ , which is the time evolution operator of the system over one period. It can thus be found as the solution of the Schrödinger equation for the time-evolution operator

$$i \frac{d}{dt} U(t, t_0) = H(t) U(t, t_0), \quad (1.2)$$

$$U(t_0, t_0) = 1, \quad (1.3)$$

evaluated after one period:

$$F_{t_0} = U(t_0 + T, t_0). \quad (1.4)$$

One can write the solution formally as

$$F_{t_0} = \mathbb{T} \exp \left( -i \int_{t_0}^{t_0+T} H(t) dt \right), \quad (1.5)$$

where  $\mathbb{T}$  refers to time ordering.

It is important to note that the Floquet operator depends on the choice of  $t_0$ . However, different choices are related by a unitary transformation:

$$F_{t_1} = U(t_1, t_0) F_{t_0} U(t_0, t_1). \quad (1.6)$$

We will refer to the choice of  $t_0$  as the choice of a *time frame* for the Floquet operator. It is analogous to the choice of a unit cell for a lattice in the Bloch theory.

## 1 Introduction

*Quasienergy and effective Hamiltonian* In analogy with the Bloch theorem, it can then be shown that any solution of the time-dependent Schrödinger equation can be written as a superposition of solutions that are eigenfunctions of the Floquet operator. Such solutions can be written as

$$\psi_\varepsilon(t) = e^{-i\varepsilon t} u_\varepsilon(t), \quad (1.7)$$

where  $e^{-i\varepsilon T}$  is an eigenvalue of  $F$ , and  $u_\varepsilon(t)$  is a function with period  $T$ .

If one considers the function  $\psi_\varepsilon(t)$  only at integer multiples of  $T$ , its time dependence resembles that of a wave function with energy  $\varepsilon$ . It is thus said to have *quasi-energy*  $\varepsilon$ . For time scales much larger than  $T$ , the evolution of a wave function is the same as that of a system governed by a stationary Schrödinger equation with the *effective Hamiltonian*

$$H_{\text{eff}} = \frac{i}{T} \log(F_{t_0}). \quad (1.8)$$

Because of the transformation Eq. (1.6), the spectrum of  $H_{\text{eff}}$  does not depend on the choice of  $t_0$ , but the eigenfunctions  $u_\varepsilon(t)$  do.

Finally, we note that all quasienergies  $\varepsilon$  can be chosen to lie in the interval  $[-\frac{\pi}{T}, \frac{\pi}{T}]$  (corresponding to the selection of the principle branch of the logarithm) and should be considered periodic on that interval. This is again in analogy with spatially periodic systems, and in fact this interval is sometimes referred to as the quasienergy Brillouin zone.

### 1.3 Random walks and quantum walks

*Random walks* A classical random walk is a random process of a walker on a one-dimensional lattice with lattice sites labeled by  $x \in \mathbb{Z}$ . The walk consists of an integer number of steps, during each of which the walker either walks to the right with probability  $p$ , or to the left with probability  $1 - p$ . We refer to the position of the walker after  $t$  steps as  $X_t$ .

For the probability distribution after  $t$  steps,  $\rho(x, t) = \Pr(X_t = x)$ , one thus obtains the recursion relation

$$\rho(x, t + 1) = p\rho(x - 1, t) + (1 - p)\rho(x + 1, t). \quad (1.9)$$

For the walker starting at site  $x = 0$ , the solution is well-known to be the binomial distribution

$$\rho(x, t) = \begin{cases} \binom{t}{(x+t)/2} p^{(x+t)/2} (1-p)^{(x-t)/2} & \text{if } x+t \text{ even,} \\ 0 & \text{otherwise.} \end{cases} \quad (1.10)$$

### 1.3 Random walks and quantum walks

*Quantum random walks* One of the basic assumptions of quantum theory is that the result of a measurement is a random process. We can thus implement a classical random walk by using quantum mechanics: We consider a quantum mechanical particle (the walker) on a one-dimensional lattice, whose state space is spanned by  $\{|x\rangle, x \in \mathbb{Z}\}$ , together with a coin, whose state space is spanned by the two states  $\{|+\rangle, |-\rangle\}$  (corresponding to “heads” and “tails”). Any state of the total system is thus given by a two component wave function  $\psi(x) = (u(x), v(x))$  by the expansion

$$|\psi\rangle = \sum_x u(x)|x\rangle|+\rangle + v(x)|x\rangle|-\rangle. \quad (1.11)$$

Instead of referring to the two systems as walker and coin, we appeal to a physicist’s intuition by regarding  $\psi$  as the wave function of a spin-1/2 particle on a lattice. Correspondingly, the two coin states will also often be referred to as “spin-up” and “spin-down” (instead of “heads” and “tails”).

Assume now that the system starts out in the state  $|\psi_0\rangle = |x=0\rangle|+\rangle$ . We then apply the following operations: We first “flip” the coin by applying a rotation of the spin:

$$R_\theta \begin{pmatrix} u(x) \\ v(x) \end{pmatrix} = \begin{pmatrix} \cos\theta & -\sin\theta \\ \sin\theta & \cos\theta \end{pmatrix} \begin{pmatrix} u(x) \\ v(x) \end{pmatrix} = e^{-i\theta\sigma_y} \begin{pmatrix} u(x) \\ v(x) \end{pmatrix}, \quad (1.12)$$

where here and in the rest of the introduction, we use  $\vec{\sigma} = (\sigma_x, \sigma_y, \sigma_z)$  to denote the vector of Pauli matrices in the  $\{|+\rangle, |-\rangle\}$  basis of the coin.

After the rotation, we apply a *spin-dependent translation operator*  $S$ , defined by:

$$S \begin{pmatrix} u(x) \\ v(x) \end{pmatrix} = \begin{pmatrix} u(x-1) \\ v(x+1) \end{pmatrix}, \quad (1.13)$$

which moves the spin-up component of the wave function to the right and the spin-down component to the left. If we now perform a measurement of the position of the walker, the walker will have performed a random walk step, having moved to the right with probability  $p = \cos^2\theta$ , and to the left with probability  $1-p = \sin^2\theta$ . A balanced random walk is obtained when choosing  $\theta = \pi/4$ . In order to perform another step, the coin must be reinitialized to  $|+\rangle$ .

## 1 Introduction

*The simple quantum walk* The idea of a *quantum walk* is repeating the two steps of rotation and spin-dependent shift without the intermediate measurement.<sup>91</sup> Because measurement is the only source of classical randomness in the previous description, it has become customary to omit the term *random* from the name.

A quantum walk in this basic form we can thus consider as a protocol for the time evolution of a spin- $\frac{1}{2}$  particle on a one-dimensional lattice, obtained by application of two unitary operations in alternation. The time evolution of the system is thus given only in discrete steps, unlike systems whose time evolution is defined by a Hamiltonian.

In a sense, quantum walks can be considered as a simplified “lattice model” for periodically driven systems, restricting the wave functions to only a finite lattice in time (with two points per period  $T$  in this case), in a similar manner as tight-binding models are simplified models for systems in a periodic potential.

The time evolution of the simple quantum walk during a whole cycle is thus given by

$$\begin{aligned}\psi(t) &= F\psi(t-1) = F^t\psi(t=0), \\ F &= SR_\theta.\end{aligned}\tag{1.14}$$

where we choose the units of time so that the period is  $T = 1$ .

In order to distinguish this time evolution from generalizations of this idea (see below), we refer to this time evolution as the *simple quantum walk* with rotation angle  $\theta$ .


*Choice of time frame* As discussed before, the quasienergy spectrum of a time evolution like Eq. (1.14) is defined unambiguously. The corresponding eigenfunctions, however, are not: As for the general case of Floquet system, there is a freedom of choice for  $F$ , corresponding to different time frames. However, while for Floquet systems governed by a time-dependent Hamiltonian  $H(t)$  we obtain a family of Floquet operators  $F_t, t \in [0, T]$ , for the quantum walk the choice is limited because time evolution is only defined in discrete steps: The two choices for the simple quantum walk are  $F_1 = SR_\theta$  and  $F_2 = R_\theta S$ .

By breaking the time evolution operator in slightly smaller pieces, more choices are possible. Considering the rotation as the product of smaller rotations, we can write the same time evolution as repeated application of  $F_3 = R_{\theta/2}SR_{\theta/2}$ . By splitting the shift operator in two



### 1.3 Random walks and quantum walks

commuting operators  $S = S_+S_-$ , where each of the two only shifts one spin species while leaving the other in place, we can also choose  $F_4 = S_+RS_-$ . The two latter choices for  $F$  are of special relevance as they imply additional symmetries on the eigenfunctions, which is play a role in Chapters 2, 3 and 4.

*The Galton board* There is an illustrative device to demonstrate the idea of a classical random walk, called the Galton board (also known as a quincunx, or bean machine), which consist of a board with interleaved rows of pins, arranged in a diagonal lattice (the term quincunx actually refers to the arrangement of five dots as on the five-side of a regular game die: , which is the arrangement repeated to form the lattice of pins on the Galton board, see Fig. 1.1). If a stream of irregular shaped objects (beans) is flowing through this arrangement, the objects will pass one pin of each row either on the left or the right, with a very high sensitivity to the precise conditions, so essentially with equal probability,  $p = 1/2$ . If the object are collected in bins after  $t$  rows, one obtains a histogram of samples from the probability distribution  $\rho(x, t)$ . The vertical axis thus represents time in this experiment.

*The optical Galton board* An analogous implementation of the quantum walk is obtained by replacing the beans with a monochromatic beam of light, and the pins with semi-transparent mirrors, so-called beam splitters. The amplitudes of two incoming wave fronts ( $u, v$ ) at 45-degree angles from both sides is related to the outgoing wave fronts at 45-degree angles ( $u', v'$ ) by the scattering matrix

$$\begin{pmatrix} u' \\ v' \end{pmatrix} = \begin{pmatrix} \cos \theta & -\sin \theta \\ \sin \theta & \cos \theta \end{pmatrix} \begin{pmatrix} u \\ v \end{pmatrix}, \quad (1.15)$$

where we took the liberty to define the phase of the incoming and outgoing modes so that this matrix is real. The angle  $\theta$  is given by the reflectivity of the beam splitter. If we arrange an array of identical beam splitters in the same manner, an incident beam on one of the first rows in the array will propagate through the lattice, performing a simple quantum walk. The state of the coin is encoded in horizontal component of the wave vector. The beam splitters perform the action of the coin operator  $R$ , while the free propagation in the space between the beam splitters leads to the shift operator  $S$ . Detecting the intensity of

## 1 Introduction

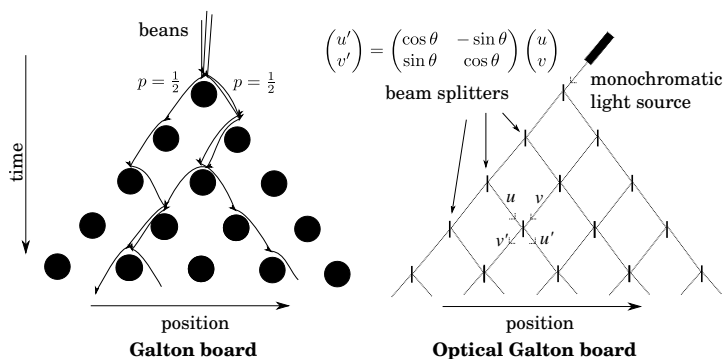


**Figure 1.1:** *Left:* The Galton board consists of pins through which beans are falling, performing a classical random walk. The number of rows of pins corresponds to the number of time steps taken in the walk. *Right:* In the optical Galton board, the beans are replaced by a monochromatic beam and the pins by beam splitters. Beams propagating to the right are considered spin-up and left-propagating beams spin-down. The mixing of the two species happens at the beam splitters, which corresponds to a rotation  $R_\theta$ , while diagonal propagation in the space between the beam splitters corresponds to a spin-dependent shift. In a “balanced” quantum walk with half-transparent mirrors, one has  $\theta = \pm\pi/4$  or  $\theta = \pm 3\pi/4$ .

the partial beams after  $n$  rows of beam splitters will thus result in the probability distributions  $(|u(x)|^2, |v(x)|^2)$  of the corresponding quantum walk. By interference measurements, one could even recover the phases, and thus obtain the function  $\psi(x, t)$ .

One might argue that this construction shows that in fact the quantum walk does not even deserve the name “quantum”, as it can be implemented using classical waves. However, it must be understood that both of the experiments presented here for the classical and quantum walk only serve as an illustration of the corresponding processes and are by no means an *efficient* implementation of either, given that the size of the physical system is proportional to the square of the number of steps. In contrast, an efficient simulation of the classical quantum walk, on a classical computer, say, only requires  $\log_2(n)$  physical objects (bits) to hold the position of the walker, and similarly, an efficient implementation of the quantum walk only requires  $\log_2(n)$  qubits.

*Differences between random walk and quantum walk* Even though the construction in the previous paragraphs suggests similarities between

### 1.3 Random walks and quantum walks

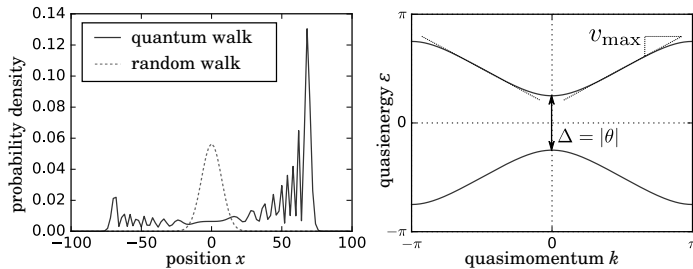


**Figure 1.2:** *Left:* Comparison of a classical random walker starting at the origin and a simple quantum walker with  $\theta = \pi/4$  and initial state  $|\psi_0\rangle = |x=0\rangle|+\rangle$ , after  $t = 100$  steps. We show the probability density  $\rho(x)$  for the classical walker, and the probability distribution for a position measurement  $\rho(x) = |u(x)|^2 + |v(x)|^2$  for the quantum walk. For both walks, we only show the probability at even lattice sites, for odd lattice sites the probability is zero. *Right:* The quasienergy band structure of the same quantum walk. The maximum propagation speed is  $v_{\max} = \pm\sqrt{2}$ , and the gap in the spectrum is given by  $\Delta = |\theta|$ .

classical random walks and quantum walks, it turns out that the two behave quite differently. To illustrate the difference, we consider the spread of the probability amplitude of a particle that starts out on a single site with spin up,  $|\psi_0\rangle = |x=0\rangle|+\rangle$ . We choose the rotation angle  $\theta = \pi/4$ . Fig. 1.2 shows the square of the probability amplitude after  $n = 100$  steps, compared to the probability distribution of a classical random walker starting at  $x = 0$ , which is  $\rho(x, t = 100)$ .

While for the random walk we obtain the familiar bell-shaped distribution of width  $\sqrt{t}$ , the quantum walk results in a relatively flat distribution, featuring oscillations, and terminated by two peaks at around  $\pm t/\sqrt{2}$ .

The long time behavior of the quantum walk Eq. (1.14) can be understood by considering its Floquet operator and corresponding quasienergy spectrum. Because this system is translational invariant, we can perform a Fourier transformation in space:

$$\psi(x, t) = \int_0^{2\pi} \frac{dk}{2\pi} e^{ikx} \psi(k, t). \quad (1.16)$$

In this basis, the shift operator  $S$  preserves  $k$  and can be written as

$$S(k) = \exp(i\sigma_z k). \quad (1.17)$$

We thus can calculate and diagonalize the Floquet operator in spin

## 1 Introduction

space.<sup>101</sup> The result can be expressed as

$$F(k) = SR_\theta = \exp(-i\varepsilon_k \hat{n}_k \cdot \vec{\sigma}), \quad (1.18)$$

and the corresponding effective Hamiltonian is thus given by

$$H_{\text{eff}} = \varepsilon_k \hat{n}_k \cdot \vec{\sigma}. \quad (1.19)$$

In this expression, the quasienergies  $\varepsilon_k$  is given by (see Fig. 1.2)

$$\varepsilon_k = \pm \arccos(\cos k \cos \theta). \quad (1.20)$$

This spectrum can be used to discuss the long-time behavior of a wave packet<sup>97</sup>: A stationary-phase approximation of a wave function that contains contribution from all  $k$  (as a very localized initial conditions does, by Heisenberg's uncertainty relation), will have most of its contribution at  $\pm v_{\text{max}}$ , which for  $\theta = \pi/4$  is given by  $v_{\text{max}} = \sqrt{2}/2$ . Besides the ballistic spread, the other striking difference between the two distributions in Fig. 1.2 is the asymmetry of the quantum walk. It is a consequence of the asymmetry of the initial condition  $|+\rangle$ , together with the fact that the quantum walk is *not* "random", i.e. Markovian, and does retain information about its past indefinitely, due to its unitary evolution. The fact that the  $|+\rangle$  state is asymmetric becomes clear in Fig. 1.1, where the initial spin is given by the direction of the initial beam.

## 1.4 Generalizations and related concepts

Above, we described the simplest version of the quantum walk, consisting of a shift and a rotation. Since, a plethora of generalizations have been considered.

A generalization in one dimension is to split the shift operator  $S$  in two operators  $S = S_+ S_-$  which only shift one spin component, leaving the other in place:

$$S_+ \begin{pmatrix} u(x) \\ v(x) \end{pmatrix} = \begin{pmatrix} u(x-1) \\ v(x) \end{pmatrix}, \quad S_- \begin{pmatrix} u(x) \\ v(x) \end{pmatrix} = \begin{pmatrix} u(x) \\ v(x+1) \end{pmatrix}. \quad (1.21)$$

Additionally, a longer sequence of different rotations can be applied. This leads to the family of *split-step quantum walks*<sup>14,101</sup> with Floquet operators given by

$$F = S_n R_{\theta_n} \cdots S_2 R_{\theta_2} S_1 R_{\theta_1}, \quad (1.22)$$

where  $S_n \in \{S_+, S_-\}$  and each  $\theta_n \in [0, 2\pi]$ . These one-dimensional walks are the main subject of study in Chapters 2, and time-dependent Hamiltonians with similar properties are studied in Chapter 3.

Generalizations to higher dimensions have also been studied.<sup>54,101</sup> A common approach is to introduce shift operators that perform the spin-dependent shift along a selected axis and applies these alternatingly.

Another generalization (in one or more dimensions) is the introduction of a coin space of higher dimension. The shift operator then typically shifts two perpendicular subspace in opposite directions. This approach is used in Chapter 2 to obtain a quantum walk with additional symmetries.

In fact, there are generalizations of the idea of a quantum walk to arbitrary graphs.<sup>60</sup> A similar approach,<sup>168</sup> which is used in the design of quantum algorithms, establishes a one-to-one correspondence between random walks (Markov processes) on any graph and a “quantized” walk on the same graph. Unlike described here, this approach is based on reflections as the basic building block, not rotations. Still, under this paradigm, the random walk on a line and the simple quantum walk described above are indeed mapped to each other.\*

Yet another modification of the quantum walk, which was considered especially in the context of the optical Galton board implementation, is the addition of non-linear operator to the time-evolution.<sup>130</sup> A modification of this nature is investigated in Chapter 4.

## 1.5 Band topology

In this thesis, we are mostly concerned with the topological properties of the band structure of quantum walks. Before we consider the peculiarities occurring in quantum walks and driven system, we quickly review the idea of topological band structures. We restrict our attention to non-interacting systems and focus mainly on one-dimensional systems.

The general idea is that a band is a periodic and continuous map from the toric Brillouin zone to the set of eigenfunctions (mathematically, elements of  $\mathbb{C}P^n$ ).<sup>†</sup> For one-dimensional two-band models like the simple

---

\*Because any rotation can be written as a product of two reflections, quantum walks with rotations and quantum walks with reflections are very similar in any case.

<sup>†</sup>This means that eigenfunctions are only defined up to a phase. This is important, because in general, one cannot make a continuous choice of phase for all  $k$ .

## 1 Introduction

quantum walk, it is the map from the unit circle of quasimomenta to spinors, which can be imagined on the surface of the Bloch sphere. The spin structure of a band can thus be envisioned as a closed path on the surface of a sphere.

Under certain conditions, mappings can be different from each other topologically, meaning that it is impossible to continuously deform one mapping into the other. For closed curves on the Bloch sphere, however, no such distinction exists: All paths on the unit sphere can be smoothly deformed into a point, and thus also into each other.

*Winding of a chiral Hamiltonian* This situation can change, however, when additional constraints are present. For instance, consider a tight-binding Hamiltonian on a bipartite lattice with no on-site energies. This means that the lattice can be divided into two sublattices  $A$  and  $B$ , and the Hamiltonian only has finite elements between the two. We can then write the Hamiltonian as

$$H = \begin{pmatrix} 0 & \tilde{H}^\dagger \\ \tilde{H} & 0 \end{pmatrix}, \quad (1.23)$$

where the subblocks of the Hamiltonian correspond to the  $A$  and  $B$  sublattice. The subblock  $\tilde{H}$  still is a matrix in position basis (ignoring for now possible further sub-structure such as spin). The structure of this Hamiltonian can be described as

$$\sigma_z H \sigma_z = -H, \quad (1.24)$$

where  $\sigma_z$  is acting on the  $A/B$  blocks. A symmetry of this sort is referred to as *chiral* symmetry.\*

We now consider the translationally invariant case, where bands can form. We write the same Hamiltonian in momentum basis:

$$H(k) = h_x(k)\sigma_x + h_y(k)\sigma_y = \begin{pmatrix} 0 & h^*(k) \\ h(k) & 0 \end{pmatrix}. \quad (1.25)$$

Then, the spinors are restricted to the equator on the Bloch sphere, as long as  $h(k) \neq 0$ . The path associated with each band will traverse this

---

\*This term is borrowed from elementary particle physics, where its occurrence in a Hamiltonian actually is related to the *handedness* of the corresponding particles. Here, the term is used because of the similar mathematical structure. For an overview over the history of the different uses of this term, we refer to the introductory chapter of Ref. 49

circle an integer number of times, and no deformation subject to the chiral symmetry restriction can change this; furthermore there even is a sense of orientation to this winding. For the underlying Hamiltonian, its two bands will preserve this distinction as long as the bands are separate, i.e. the gap does not close,  $h(k) \neq 0$ .

To capture this idea in mathematical terms, note that an eigenvector  $\xi_k = (u(k), v(k))$  of the Hamiltonian (1.25) will always satisfy  $|v(k)/u(k)|^2 = 1$ , (the stereographic projection of the equator of the Bloch sphere is the unit circle). Thus, we can write the integral

$$v = \int \frac{dk}{2\pi i} \partial_k \log(v(k)/u(k)), \quad (1.26)$$

which, according to the Cauchy integral theorem, will give the number of times  $v/u$  winds around the origin, or equivalently (by stereographic projection), how often  $\xi_k$  winds around the north-south axis of the Bloch sphere. In this two-band example, the other band is given by  $\bar{\xi}_k = (u_k, -v_k)$ , and has the same winding number. Because  $v/u = h/|h|$ , the winding can also be found directly from the Hamiltonian:

$$v = \frac{1}{2\pi i} \oint \frac{dh}{h} = \int \frac{dk}{2\pi i} \partial_k \log(h(k)), \quad (1.27)$$

*Symmetry classes* In one dimension, topological distinction of bands can thus only occur under the assumption of symmetries. These symmetries are assumed to act locally: We require that they only act on the spin subspace.\* Usual unitary symmetries which commute with the Hamiltonian are generally not of interest, they only lead to decoupled blocks of the Hamiltonian which can be considered individually. But there are other symmetries, which anticommute with the Hamiltonian, or are antiunitary. That leaves three possibilities: *Time-reversal symmetry*  $T$  (antiunitary, anticommuting), *particle-hole symmetry*  $P$  (antiunitary, commuting), and *chiral symmetry*  $\Gamma$  (unitary, anticommuting).<sup>9,150</sup> The antiunitary symmetries can either square to 1 or  $-1$ , and the presence of two of such symmetries dictates the presence of the third;† this results

---

\*In some systems, like graphene, a chiral symmetry emerges due to a sublattice symmetry. Then, the chiral symmetry operator involves two neighboring sublattice sites, and thus is only “almost” local.

†Also, not more than one of each of the symmetries can be present. E.g. if there are two time-reversal symmetries  $T_1$  and  $T_2$ , then  $T_1 T_2$  is a unitary symmetry of the Hamiltonian, which we excluded.

## 1 Introduction

in the existence of ten different symmetry classes, of which five turn out to allow topological distinctions in one dimension. Chapter 2 considers all of these, while in the rest of the introduction, we only consider classes AIII and BDI (see below) as examples.

Finally, we remark that the names of the symmetry operators hint to certain physical mechanism that ensure them. However, in this thesis, most models are rather artificial, so that the names of the symmetries should be considered historical, and their mathematical properties should be taken as their definition independent of their origin.

Consider the Hamiltonian Eq. (1.25). It can have all three symmetries: It will always have a chiral symmetry represented by the operator  $\Gamma = \sigma_z$ :

$$\sigma_z H(k) = -H(k) \sigma_z. \quad (1.28)$$

If this is the only present symmetry, the Hamiltonian is said to belong to symmetry class AIII. If furthermore,  $h(k) = h^*(-k)$ , the system also has a particle-hole symmetry  $P = K$ , which is complex conjugation in position basis:

$$H^*(-k) = H(k). \quad (1.29)$$

Note that complex conjugation in position basis involves  $k \rightarrow -k$  in momentum basis. This particle-hole symmetry operator  $P$  is of the kind  $P^2 = 1$ . Furthermore, because  $\Gamma$  and  $P$  are present, then also  $T = \Gamma P = \sigma_z K$  is a time-reversal symmetry of the system, and in this case is of type  $T^2 = 1$ . This class is referred to as BDI and as we will see shortly, the simple quantum walk belongs to this class.

However, so far, we have discussed the symmetries and band topology of time-independent Hamiltonians. The same classification can be applied to the quasienergy bands of a Floquet system, but the role of the symmetries has to be carefully re-evaluated: Firstly, it is not immediately clear how the presence of a discrete symmetry in the effective Hamiltonian is caused by certain symmetries in the underlying time-dependent Hamiltonian. Secondly, even if such a symmetry exists, because the eigenfunctions depend on the choice of the time frame, the symmetries and corresponding topological numbers may also depend on the time frame. This allows for a somewhat richer classification scheme of the topology of driven systems and is the main subject of investigation in Chapters 2 and 3.



*Symmetry and topology of the simple quantum walk* To illustrate these points, we discuss the topological properties of the simple quantum walk. The Floquet operator is given by

$$F = S e^{-i\theta\sigma_y} \quad (1.30)$$

As we can check immediately, the effective Hamiltonian has a particle-hole symmetry  $P = K$ , as can be seen from

$$F^* = F, \quad (1.31)$$

because  $S$  is real in position basis (it only has matrix elements 0 and 1). It follows that

$$H_{\text{eff}}^* = -H_{\text{eff}}. \quad (1.32)$$

It turns out that the same system also has a chiral symmetry.<sup>14,14,101</sup> However, in the effective Hamiltonian presented above, it is “hidden”. Namely, when changing the time frame to

$$F = R_{\theta/2} S R_{\theta/2}, \quad (1.33)$$

we can see by a quick calculation that

$$\sigma_x F \sigma_x = F^{-1} \Rightarrow \sigma_x H_{\text{eff}} \sigma_x = -H_{\text{eff}}, \quad (1.34)$$

so that chiral symmetry is given by  $\Gamma = \sigma_x$ . Particle-hole symmetry is still given by  $K$ ; consequently, a time-reversal symmetry is also present. The symmetry class this effective Hamiltonian thus is BDI, and by a simple change of basis, we could write it in the form of Eq. (1.25).

The winding number of this effective Hamiltonian can be found by direct calculation, and turns out to be  $\nu = \text{sgn}\theta$ .\*

If we try to find the “hidden symmetry” in the original time frame, we can use the fact that time frames are connected by unitary transformations. We can reconstruct the action of  $\Gamma = \sigma_x$  and find the “chiral symmetry operator” in the original basis:  $\Gamma = R_{-\theta/2} \sigma_x R_{\theta/2}$ . This operator is not a useful symmetry operator: It explicitly contains the parameter  $\theta$ , and thus it is not sensible to compare the winding numbers of

---

\*The sign is actually not well-defined, as it depends on the basis transformation used to bring  $H_{\text{eff}}$  to a standard form. For discussion of this matter we refer to the appendix of Chapter 2.

## 1 Introduction

Hamiltonians with different values of  $\theta$ , furthermore, adding any inhomogeneities or disorder to  $\theta$  seems to break it. In the symmetrized time frame Eq.(1.33), however, these problems do not apply. We thus say that the simple quantum walk belongs to symmetry class BDI because *there exists one time frame* in which the effective Hamiltonian has the required symmetries.

Finally, we note that in the second symmetrized time frame mentioned above, namely  $F = S_+RS_-$ , the same chiral symmetry  $\Gamma = \sigma_x$  holds; the winding number in this time frame however is always  $\nu = 0$ , independent of  $\theta$ . We thus see that the choice of time frame is relevant.

## 1.6 Bulk-boundary correspondence

The most interesting consequence of band topology occurs when two large (so that bands can form) systems are interfaced at a common boundary. The general principle of the *bulk-boundary correspondence* predicts that at such an interface, bound states of a certain type must always exist even when both systems have no extended states at that energy and the topological number is different for both systems.

In general, the features of such bound states depend on the dimensionality of the problem and on the symmetries involved. In one dimension, such bound states are located precisely at zero energy (which is a special energy, because it is singled out by chiral or particle-hole symmetry). These states, often called *Majorana zero modes*, have been the subject of much interest recently for their robustness: not only is their presence guaranteed independent of the details of the boundary, and also not destroyed by the presence of disorder, but additionally their energy is pinned to a fixed value. This *topological protection* makes these states interesting for use as storage of quantum information (qubits).

*The bulk-boundary correspondence in one-dimensional chiral systems*  
Because the later chapters make much use of the bulk boundary correspondence, we shall sketch here, as an example, how the bulk-boundary correspondence emerges for two-band Hamiltonians with chiral symmetry. We consider a setup where the lattice is divided into two *bulk domains*  $A$  and  $B$ , in which the Hamiltonian is constant in space, with different parameters, so that it can be described by two translationally invariant Hamiltonians  $H_{A,B}(k)$ . In between, in the *boundary region*,

## 1.6 Bulk-boundary correspondence

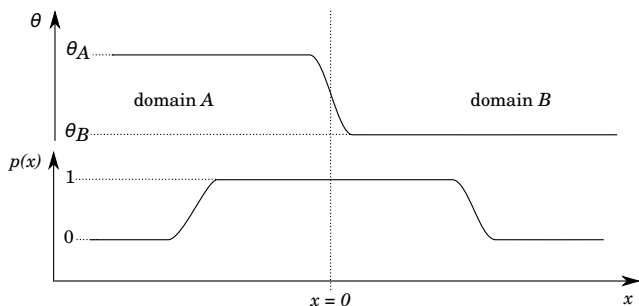


**Figure 1.3:** At a domain boundary, the Hamiltonian, parametrized by the parameter  $\theta$ , varies between two different values  $\theta_A$  and  $\theta_B$ , and is translationally invariant in the two bulk domains. If the two Hamiltonians are topologically different, protected zero modes are expected in the region where the function  $p(x)$  is finite, which is the essence of the bulk-boundary correspondence.

the Hamiltonian interpolates between the two domains in an arbitrary way (see Fig. 1.3), with the restriction, however, that the Hamiltonian of the total system still obeys the chiral symmetry, so that we can write it as:

$$H = \begin{pmatrix} 0 & h^\dagger \\ h & 0 \end{pmatrix}, \quad (1.35)$$

where  $h$  is a matrix acting on position space only, and its matrix elements  $h_{xx'}$  are local: We require that  $h_{xx'}$  decays exponentially as  $|x - x'| \rightarrow \infty$ , and that  $h$  approaches translational invariance deep in the domains.

*The flat-band Hamiltonian* The object of consideration now is a deformed version of  $H$ , the *flat-band Hamiltonian*  $Q$ , given by

$$Q = \text{sign}H, \quad (1.36)$$

which is obtained by deforming all positive eigenvalues of  $H$  to +1 and all negative eigenvalues to -1, and leaving zero eigenvalues at zero. For the bulk Hamiltonians, this corresponds to rectifying the loop  $h(k)$  to lie on the unit circle,  $h(k) \rightarrow q(k) = h(k)/|h(k)|$ , which does not change its winding number. We thus can write the operator for the setup including the boundary as

$$Q = \begin{pmatrix} 0 & q^\dagger \\ q & 0 \end{pmatrix}, \quad (1.37)$$

## 1 Introduction

where the operator  $q$  acts on space only. A crucial important property of  $Q$ , which we shall not prove here, is that, like  $H$ , its matrix elements decay in real space exponentially, i.e.  $q_{xx'} = O(e^{-\xi|x-x'|})$  as  $|x-x'| \rightarrow \infty$  for some decay length  $\xi$ .\*

Consider now an eigenfunction  $\psi = (u, v)$  of  $Q$  with eigenvalue  $\pm 1$ :

$$qu = \pm v, \quad q^\dagger v = \pm u. \quad (1.38)$$

Then,

$$q^\dagger qu = u, \quad qq^\dagger v = v \quad (1.39)$$

And thus,  $u$  is an eigenvector of  $q^\dagger q$  while  $v$  is an eigenvector of  $qq^\dagger$ , both with eigenvalue 1.

Eigenfunctions of  $Q$  with eigenvalue 0, on the other hand, can be chosen to have either  $v = 0$  or  $u = 0$ , and thus are eigenfunctions of the chiral operator  $\sigma_z$  at the same time. We thus distinguish zero modes by their *chirality*  $n$ ,  $\sigma_z \psi = n\psi$ , where  $n = \pm 1$ .

*Counting the zero modes* We can thus write down the *total chirality*, i.e. the sum of the chiralities of all the zero modes of  $Q$ , as

$$n = \dim \ker q^\dagger q - \dim \ker qq^\dagger \quad (1.40)$$

( $\dim \ker$  denotes the dimension of the kernel, in other words, the number of linearly independent zero eigenfunctions) and because we just saw that the eigenvalues of  $qq^\dagger$  and  $q^\dagger q$  only take values 0, 1, this can be expressed as traces:

$$n = \text{tr}(1 - q^\dagger q) - \text{tr}(1 - qq^\dagger) = \text{tr}(qq^\dagger - q^\dagger q). \quad (1.41)$$

Only zero modes of  $Q$  contribute to exactly one of the two traces, depending on the chirality. We immediately see that in any finite system (i.e. with periodic boundary conditions), the total chirality  $n = 0$ , by cyclic invariance of the trace. For the infinite line, the mathematical situation is more complicated and the result can be finite.<sup>142</sup>

---

\*In fact, an algebraic decay  $|x-x'|^\alpha$  with  $\alpha < -1$  is sufficient<sup>95</sup>; but fast decay often holds and makes for somewhat easier intuition of the proof.

## 1.6 Bulk-boundary correspondence

*Zero modes in a region* We can modify the formula to count only those zero modes that have support in the boundary region. For that, we introduce the operator

$$P = \sum_x p_x |x\rangle \langle x|, \quad (1.42)$$

where (see Fig. 1.3)

$$p_x = \begin{cases} 1 & \text{close the boundary region} \\ \rightarrow 0 & \text{as } |x| \gg \xi, \text{ far in the domains.} \end{cases} \quad (1.43)$$

This allows us to define the chirality of that region as

$$n = \text{tr}(qq^\dagger - q^\dagger q)P. \quad (1.44)$$

The effect of the operator  $P$  is that eigenfunctions of  $Q$  only contribute according to their weight in the region where  $p_x$  is finite, so that zero modes in the region where  $p_x = 0$  are not counted.

In position space we can then write

$$n = \sum_{xx'} (q_{x'x}^* q_{x'x} - q_{xx'}^* q_{xx'}) p_{x'} = \sum_{xy} q_{x+y,x}^* q_{x+y,x} (p_{x+y} - p_x), \quad (1.45)$$

and because  $q_{x+y,x}$  decays, there is no contribution for large  $y$ . This means that there is no contribution for  $x$  close to the boundary, because  $p_x - p_{x+y} = 1 - 1 = 0$  for small  $y$ . We only get contributions where  $p$  varies, which is in the bulk. This allows us to obtain an expression which only involves the bulk Hamiltonians and is independent of the exact properties of the boundary.

In the bulks,  $q$  is translationally invariant, and we can write  $q_{xx'} = q_{A,x-x'}$  where  $p$  varies from zero to one, and  $q_{xx'} = q_{B,x-x'}$  where  $p$  varies back to zero. Then we can write\*

$$n = \sum_{xy} q_{x+y,x}^* q_{x+y,x} (p_{x+y} - p_x) = \sum_y y q_{A,y}^* q_{A,y} - \sum_y y q_{B,y}^* q_{B,y}. \quad (1.46)$$

---

\*We used the following telescoping formulas:

$$\sum_{x \ll 0} p_x - p_{x+1} = p_{-\infty} - p_0 = -1, \quad \text{thus} \quad \sum_{x \ll 0} p_x - p_{x+y} = -y.$$

for all not too large  $y$ ; and a similar expression for  $x > 0$ . The fact that we then can also extend the sum over  $y$  to infinity requires the decay of  $q$ .

## 1 Introduction

Using the Fourier transform  $q_{A/B,y} = \int q_{A/B,k} e^{iky} (dk/2\pi)$ , we can finally write this as  $n = \nu_B - \nu_A$ , where

$$\nu_{A/B} = -\sum_y y q_{A/B,y} q_{A/B,y}^* = -i \int \frac{dk}{2\pi} q_{A/B,k}^* \partial_k q_{A/B,k}, \quad (1.47)$$

which is the winding number of  $q(k)$ , and thus  $h(k)$  defined in Eq. (1.27). Thus we conclude that if the winding number of  $q(k)$ , and thus of  $h(k)$ , changes by  $\delta\nu$  across a domain boundary, the total chirality of the states in the boundary is indeed given by  $\delta\nu$ , and especially, the number of zero modes in the boundary is at least  $|\delta\nu|$ .

*Bulk-boundary correspondence in Floquet systems* The bulk-boundary correspondence also applies to effective Hamiltonians, but is not sufficient. The crucial difference is the definition of  $Q$ : While for stationary Hamiltonians, the sign function is defined unambiguously, effective Hamiltonians are defined only up to multiples of  $2\pi$ , which makes the distinction arbitrary. This also leads to the possibility of bound states at quasienergy  $\varepsilon = \pi = -\pi$  which are protected by symmetry (e.g. in class BDI as discussed above, they can carry chirality). In fact, Floquet systems have been found where the classification of the effective Hamiltonian predicts no bound states, while numerical or optical simulations show protected edge modes.<sup>99,149</sup>

How to classify the topology of driven systems beyond the bands of an effective Hamiltonian has been the subject of a lot of recent research and is addressed in Chapters 2 and 3 in this thesis.

## 1.7 Quantum algorithms

The idea of quantum walks have been generalized to arbitrary bipartite graphs (or in fact any graph, using its bipartite double cover)<sup>168</sup>, which allows the design of quantum algorithms that solves computational problems represented by such graphs.

Even though such algorithms are not the main topic of this thesis, they are a large field of application of quantum walks, and furthermore can often be understood in terms of the properties of quantum walks that we discussed above. In this section, we thus take a small detour and consider one of these algorithms, first presented in Ref. 162, and highlight their connection to topology.

*Quantum search on the hypercube* The algorithm we discuss solves the same problem as the famous Grover search algorithm.<sup>72</sup> In the problem, we want to find the solution to the problem  $f(x^*) = 0$ , where  $x^* \in \{0, 1\}^n$  i.e.  $x$  is a bit string of length  $n$ . The function  $f$  is not restricted, but we assume the solution  $x^*$  to be unique.

The computation is performed by a quantum walk on the hypercube graph, formed by possible solutions  $x$ . The walker's position thus can be any bit string  $x$  of length  $n$ , and during one step, the walker is allowed to move to any bit string  $x'$  when  $x$  and  $x'$  only differ by a bit flip at one position, (see Fig. 1.4 for an illustration with  $n = 3$ ).

*The oracle* The evaluation of the function  $f(x)$  is performed by an oracle  $O$ . This oracle is an additional unitary evolution of the walker which “marks” the solution of  $f(x) = 0$  by changing the phase of the walkers wave function on these points by  $\pi$ .<sup>\*</sup> We thus have

$$O = 1 - 2|x^*\rangle\langle x^*| \quad (1.48)$$

For definiteness, we can even assume that the solution is  $x^* = 00\dots 0$ , because except for the application of the oracle, all parts of the algorithm are invariant under bit flips of the labels of the vertices, as will become apparent immediately.

*The quantum walk on the hypercube* The generalization of the one-dimensional quantum walk to this graph is rather straight-forward: Because at each time there are  $n$  possible directions for the walker to go, we require an  $n$ -dimensional internal coin space (not a two-component spinor, as for the one-dimensional walker).

The coin rotation  $R$  must be a unitary on that space, and should be invariant under bit flips. We could use a rotation around the symmetric state  $|s\rangle$ , defined by

$$|s\rangle = \frac{1}{\sqrt{n}} \sum_{i=1}^n |i\rangle, \quad (1.49)$$

which can be written as

$$R_\theta = e^{-i\theta} |s\rangle\langle s| + e^{i\theta} (1 - |s\rangle\langle s|), \quad (1.50)$$

---

<sup>\*</sup>It must be understood that for the implementation of such an oracle, it is not necessary to know the target state  $x^*$  explicitly; In fact, if  $f$  can be computed efficiently with classical gates, the oracle can be implemented efficiently using quantum gates.

## 1 Introduction

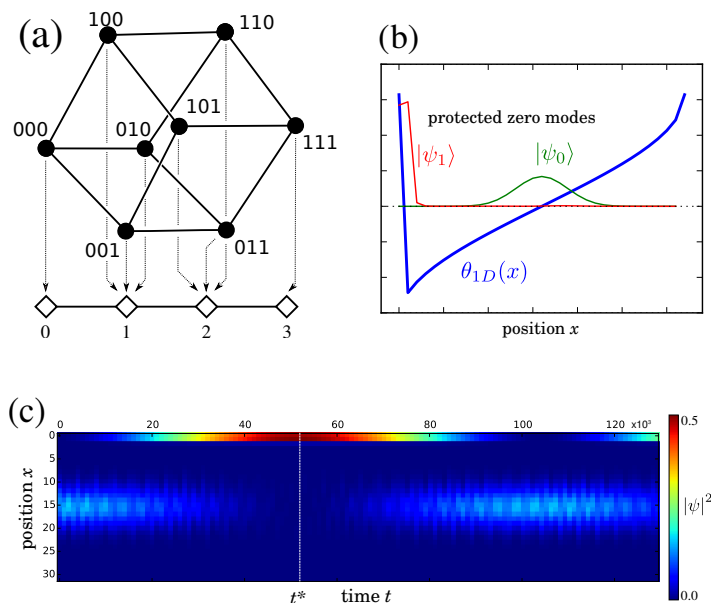


**Figure 1.4:** (a) The three-dimensional hypercube is mapped to a one-dimensional quantum walk by joining states which have the same distance to the oracle state  $|0\rangle$ . (b) The one-dimensional quantum walk has an effective  $\theta_{1D} = \arcsin(1 - x/n)$ . The oracle changes  $\theta_{1D}(x=0) = -\pi$  to  $\pi$ . This results in two bound states:  $|\psi_0\rangle$ , located around  $x = n/2$ , which corresponds to the totally delocalized state on the original hypercube, and  $|\psi_1\rangle$ , localized around the oracle state. The states are shown for  $n = 32$ . (c) The algorithm works by a beating between the initial state and the oracle state. We show this oscillation for  $n = 32$ . When measuring the position of the walker at time  $t = t^*$ , the probability of measuring the oracle state is almost 0.5.

and in order to achieve a maximal spreading speed, we can choose  $\theta = \pi/2$ . In fact, in the original description, the coin is chosen as a reflection around  $|s\rangle$  instead, which differs from  $R_{\pi/2}$  by a factor  $i$ .

The shift step then is a coin-dependent shift in the direction in which the coin is pointing, in other words, if the coin state is  $|i\rangle$ , the  $i$ th bit of  $x$  is flipped.

The algorithm then proceeds by initializing the walker in a equal superposition of all possible states and then performing a quantum walk, applying

$$F = OSR \quad (1.51)$$

repeatedly. After  $t = \frac{\pi}{2} \sqrt{2^n}$  repetitions, the position of the walker is



measured, and will result in the state marked by the oracle with high probability (almost 0.5).

*Projection to one dimension* The mechanism underlying this surprising result can be understood by projecting the walk on the hypercube to a one-dimensional walk on  $n + 1$  sites and two-dimensional coin (see Fig. 1.4a), where the position denotes the distance to the oracle state (if  $x^* = 00\dots 0$ , this is the number of 1's in the bit string, see Fig. 1.4) and the coin state is projected to either pointing towards or away from the oracle state. Omitting the action of the oracle, the result is a simple quantum walk, albeit with site-dependent rotation angle:

$$\theta_{1D} = \arcsin(1 - 2x_{1D}/n), \quad (1.52)$$

where  $x_{1D}$  labels the sites of the reduced walk, see Fig. 1.4b.

*Topological bound states in 1D walk* Because the simple quantum walk changes its bulk winding number at  $\theta = 0$ , it can be seen that this 1D walk features a topological phase transition at  $x_{1D} = n/2$ , and a corresponding chiral bound state is expected. In fact, this “bound state” is simply the result of projecting the equal superposition of all starting positions onto the 1D walk; this is just the initial condition of the described algorithm, and it in fact can be seen to be a zero-energy eigenstate of the system without the oracle.

We now consider the changes to the 1D walk when introducing the oracle operator. The oracle only acts on the target state, which is mapped to the state  $x_{1D} = 0$  and in fact in the one-dimensional projected quantum walk, it turns out to be a change of the rotation angle  $\theta_{1D}$  by  $\pi$ . This leads to the formation of a second topological phase transition, and a corresponding bound state.

The working of the algorithm is now clear: Because of the finite distance between the two bound states, they have an exponentially small, but finite overlap, leading to a splitting in quasi-energy  $\Delta\epsilon \propto 2^{-n/2}$ , so that the application of the effective Hamiltonian leads to a very slow quantum beating between the two bound states at zero energy. The algorithm terminates after half a beating period, when the walker is in the bound state exponentially localized around the oracle state, see Fig. 1.4c.

## 1.8 This thesis

We finally give a short overview over the topics and main results of each of the following chapters.

### Chapter 2

Besides considering winding numbers of the bulk, it is also possible to characterize the topological quantum numbers of band insulators by calculating the scattering matrix of a half-infinite insulator at the energies of interest.<sup>65</sup> This matrix is directly related to the bound states emerging at an interface of two such systems, and can thus be used to classify the topological properties of the Hamiltonian, in accordance with the bulk-boundary correspondence. In fact, depending on the symmetries of the system, the topological quantum number at a certain energy can be expressed in terms of the determinant, trace, or Pfaffian of the scattering matrix.

In this chapter, we extend this approach to the Floquet scattering matrix of quantum walks, immediately identifying expressions for the additional quantum numbers required for Floquet systems. We use this result to map out the topological phase diagram of several quantum walk protocols with different symmetries.

### Chapter 3

The Su-Schrieffer-Heeger model (SSH model) is a one-dimensional tight binding model with alternating hopping strengths  $u$  and  $v$ , originally devised to model the electronic structure of polymers with conjugated  $\pi$ -bonds. With fixed  $u, v$ , this system forms a one-dimensional topological insulator with chiral symmetry.

When driving the hopping strengths periodically in a symmetric way, the system becomes a topological Floquet insulator, with chiral symmetry still present. The Floquet operator of this system is very similar to that of quantum walks, and can in fact be mapped to quantum walks if the time-dependence of  $u(t), v(t)$  is chosen piecewise constant.

In this chapter, we study the topological properties and bulk-boundary correspondence of the driven SSH model and find that in order to establish a bulk-boundary correspondence for both zero and  $\pi$ -quasienergy bound states, we need to calculate the winding number of the Floquet

operator in two different time frames, or, equivalently, consider the time evolution operator  $U(T/2, 0)$  which connects the two time frames.

## Chapter 4

In this chapter, we consider the simple quantum walk as presented in the introduction. However, we introduce an important modification, which is a non-linear self-interaction of the walker. To be precise, the local spin density  $M(x) = \psi^\dagger(x)\sigma_z\psi(x)$  of the walker is taken to lead to a correction to the rotation angle  $\theta(x) = \theta_0 + \delta\theta(M(x))$  in the next time step.

This self-interaction makes the time evolution in the bulk nonlinear, and a description in terms of a single particle Floquet operator is not longer possible. However, the interaction is chosen so that topologically protected bound states, which are present at domain boundaries in the linear model, are insensitive to this non-linearity, meaning that they still are a steady state solution of the non-linear time evolution.

We show that furthermore in this model, numeric simulation suggests that some of these modes are in fact attractive fixed points of the dynamics, meaning that independent of the initial conditions, the system approaches the same stable state at finite times. We corroborate this behavior by considering the non-linear Dirac equation obtained as a continuum approximation of the quantum walk for long wavelengths.

## Chapter 5

In this chapter we consider a driven system which is not driven periodically, but instead we consider a quench, where a parameter is varied from  $-\infty$  to  $\infty$ , crossing a phase transition in between.

The system under consideration is a generalization of the single electron emitter,<sup>30,31,52,64,121,136</sup> where a quantum dot is coupled to a one-dimensional lead. The dot is assumed to have a bound state well below the Fermi energy  $E_F$ , which is thus occupied. A plunger gate is then used to control the energy of the bound state, moving it well above the Fermi energy. While the energy of the bound states crosses  $E_F$ , the particle will tunnel from the quantum dot and enter the lead as a localized excitation above the Fermi surface. Surprisingly, it has been recognized that this simple scheme to emit a single electron on top of a Fermi surface is very noiseless, in fact, at zero temperature and in

## 1 Introduction

the limit of constant derivative of the energy of the bound state, the final state of the lead is precisely the ground state of the lead, with one particle added above the Fermi surface. Thus, even though the system is explicitly time dependent and the lead is assumed gapless, no additional particle-hole pairs are created.

In this chapter, we consider a generalization of this scheme to superconducting systems. Here, we change the phase across a topological Josephson junction as a function of time, thus driving the system through a fermion parity switch. Similarly, this leads to the emission of a particle, which now, due to the presence of superconductivity, will be a Bogoliubov quasiparticle, i.e. a coherent superposition of electron and hole.

We solve the scattering problem analytically for a minimal model and find again that no additional particle-hole pairs are created in the lead. Additionally, we give expressions for the charge of the emitted quasiparticle, which in general depends on both the coupling to the lead as well as the speed of the sweep. We find that for very slow (adiabatic) sweeps, the emitted particle is always either an electron or a hole, and that in order to obtain equal superposition, a very special coupling, a *Majorana filter*, is required.

## Chapter 6

In this chapter, unlike the previous chapters, we consider a classical transport problem of a solid state system. The theoretical issue considered, inspired by experiments that are also described in detail in this chapter, is that of magnetotransport in a hexagonal indium antimonide nanowire, which features strong spin-orbit coupling. Experimentally, the spin-orbit interaction strength can be determined by measuring the so-called weak localization and weak antilocalization, which are quantum corrections to the conductivity that depend on a small magnetic field in a characteristic manner.

However, the relation between magnetic field dependence and resulting spin-orbit strength estimates depend on the geometry of the problem. Because applying results for two-dimensional wires appeared as an oversimplification for the presented experiments, we used Monte Carlo simulation and the quasi-classical technique to model the three-dimensional geometry of the hexagonal nanowires.

The results of the simulation are used to interpret the experimental

data and furthermore explain an observed independence of weak localization on magnetic field direction as a coincidence for the parameters of the examined samples.

In regimes not accessible by current experiments, the simulations predict an interesting dependence of the weak localization corrections on the ratio  $W/l_e$  with a fractional exponent, where  $W$  is the radius of the wire and  $l_e$  is the electronic mean free path.

